ELSEVIER

Journal of Nuclear Materials 307–311 (2002) 871–875

journal of nuclear materials

www.elsevier.com/locate/jnucmat

⟨1 0 0⟩-Loop characterization in α-Fe: comparison between experiments and modeling

J. Marian [a,b], B.D. Wirth [a,*], R. Schäublin [c], J.M. Perlado [b], T. Díaz de la Rubia [a]

[a] *Chemistry and Materials Science Directorate, Lawrence Livermore National Laboratory, P.O. Box 808, L-353, Livermore, CA 94550, USA*

[b] *Instituto de Fusión Nuclear, Universidad Politécnica de Madrid, C/José Gutiérrez Abascal, 2 Madrid 28006, Spain*

[c] *CRPP, Fusion Technology-Materials, École Polytechnique Fédérale de Lausanne, CK-5232, Villigen PSI, Switzerland*

Abstract

Ferritic/martensitic steels considered as first-wall candidate materials for fusion reactors experience significant radiation hardening at temperatures below ~400 °C. Experimental evidence suggests that the observed defects are large interstitial dislocation loops with Burgers vector $b = \langle 1\,0\,0\rangle$ and $b = \frac{1}{2}\langle 1\,1\,1\rangle$. In this work, the atomic character of $\langle 1\,0\,0\rangle$ and $\frac{1}{2}\langle 1\,1\,1\rangle$ loops is investigated with molecular dynamics simulations and the atomic configurations are used to calculate the defect image contrast through direct simulation of TEM images. The simulated images are subsequently compared with actual TEM micrographs of irradiated ferritic materials and are in very good qualitative agreement, providing strong indication that the observed $b = \langle 1\,0\,0\rangle$ loops are interstitial in nature.

1. Introduction

Ferritic/martensitic steels are being considered as first-wall candidate materials for fusion reactors due to their excellent radiation damage resistance and low activation under neutron irradiation conditions. It is known, however, that significant hardening occurs at temperatures below ~400 °C that may result in embrittlement of the material [1]. Hardening is believed to arise from the formation of voids, precipitates and loops under irradiation that pin and may also decorate dislocations, thereby impeding their glide during deformation. A number of experimental studies, performed at higher temperatures, in ferritic alloys have shown the existence of large interstitial loops in the bulk, which may provide a significant contribution to the hardening caused during irradiation at lower temperatures [1–5]. The population of dislocation loops exhibits both 1/2(1 1 1) and (1 0 0) Burgers vectors, with a predominance of (1 0 0) loops. It is believed, but not confirmed that these loops are interstitial in nature [2–5].

Both experimental [2–5] and from atomistic simulations [6], have confirmed the stability of $\frac{1}{2}\langle 1\,1\,1\rangle$ and $\langle 1\,0\,0\rangle$ loops in ferritic materials. Molecular dynamics (MD) simulations of high-energy cascades in Fe have revealed the formation of small, one-dimensionally mobile, $\frac{1}{2}\langle 1\,1\,1\rangle$ clusters following cascade collapse within a few picoseconds after the initiation of the event [7,8]. However, these features are sub-nanometer in size and their detection by experimental means is limited by the time and spatial scales involved. $\langle 1\,0\,0\rangle$ loops, on the other hand, have been proposed to form from the direct interaction of these small, cascade-produced, $\frac{1}{2}\langle 1\,1\,1\rangle$ clusters [3,9] and grow by the biased absorption of $\frac{1}{2}\langle 1\,1\,1\rangle$ loops to TEM visible sizes [9]. The great advantage of the MD treatment is that, due to its fully atomic resolution, unequivocal determination of loop Burgers vectors and habit planes is possible.

The main objective of this work is to investigate the correlation between dislocation loops produced by MD simulations and their observation in TEM by generating equivalent, conventional TEM (CTEM) images and assess experimental limitations in the observation of small

* Corresponding author. Tel.: +1-925 424 9822; fax: +1-925 423 7040.

E-mail address: wirth4@llnl.gov (B.D. Wirth).

0022-3115/02/$ - see front matter
PII: S0022-3115(02)01158-3

defect clusters. The weak beam technique [10] seems most appropriate in the case of small defects such as these, as it provides an improved spatial resolution and signal-to-background ratio over the usual bright/dark field mode of imaging in TEM, as well as a framework for direct comparison with actual experimental micrographs. Thus, by using a *virtual* electron microscope, this work tries to partially bridge the gap that exists between multiscale modeling and experiments within the study of radiation damage effects in metals.

2. CTEM image simulation method

The CTEM images of the dislocation loops are simulated using the multislice method [11] to obtain their weak beam image at 200 kV. This is performed with the EMS software package [12]. The most relevant parameter in this type of simulation is the objective aperture size. Ideally, for CTEM, and more precisely for weak-beam image simulation, the sample should be more than 10 nm thick to avoid surface effects, and thinner than 80 nm to reduce anomalous absorption, which arises from inelastic scattering of the electrons, that would result in a blurry image [13].

Details on the main elements of the approach are given elsewhere [14]. The sample obtained from MD simulations is cut perpendicular to the electron beam direction in slices 0.2 nm thick. The sample is in all cases cut into 100 slices that are roughly 10 nm on a side and contain approximately 2000 atoms. The diffraction condition is selected by the beam direction, parallel to the cutting direction, in order to isolate the systematic row defined by the chosen diffraction vector **g**. In this work the diffraction vector was picked to be $\mathbf{g} = (200)$ and the diffraction condition was **g**(4.1**g**). The parameters used to obtain the images are similar to those of modern microscopes operated at an acceleration voltage of 200 kV.

3. Atomistic modeling

In order to have a minimum 10 nm thickness in the simulation box, super-cells larger than 20 nm in dimension are needed, with the defect located close to the center of the box. This implies simulations involving more than one 1 million atoms. For the image simulation conditions used here ($\mathbf{g} = (200)$, **g**(4.1**g**) and 200 kV electron beam energy), we have used $80a_0 \times 80a_0 \times 80a_0$ super-cells, where a_0 is the α-Fe lattice parameter (2.8665 Å), i.e. a cubic box of 22.9 nm side containing 1 024 000 lattice sites. The simulations were carried out with the massively parallel MDCASK code [16], using the Ackland version of the Finnis-Sinclair potential to describe the interatomic interactions in Fe [17]. After inserting interstitial dislocation loops with Burgers vectors and habit planes of $\frac{1}{2}\langle 1\,1\,1\rangle\{1\,1\,0\}$, $\langle 1\,0\,0\rangle\{1\,1\,0\}$ or $\langle 1\,0\,0\rangle\{1\,0\,0\}$, the simulation cell was equilibrated for ~10 ps at a very low temperature (~10 K), followed by heating to 100 K and a numeric quench or a conjugate-gradient minimization to obtain the final relaxed structure.

The most stable configurations for each kind of loop ($\frac{1}{2}\langle 1\,1\,1\rangle\{1\,1\,0\}$, $\langle 1\,0\,0\rangle\{1\,1\,0\}$ or $\langle 1\,0\,0\rangle\{1\,0\,0\}$) were seen to correspond to *magic*-shape clusters, i.e. interstitials arranged in polygon-shaped clusters whose sides are aligned with the corresponding close-packed directions on each specific habit plane. A brief description of loop generation is provided below.

Introduction of $\frac{1}{2}\langle 1\,1\,1\rangle\{1\,1\,0\}$ and $\langle 1\,0\,0\rangle\{1\,1\,0\}$ loops was performed by replacing a $\{1\,1\,0\}$ plane of atoms, of hexagonal or rhombic shape, by two identical, consecutive platelets with the same size and shape. To obtain the appropriate Burgers vector, we shear one platelet of atoms with respect to the other. This shear is along a $[0\,0\,1]$ direction for $\frac{1}{2}\langle 1\,1\,1\rangle$ loops and along $[1\,1\,0]$ for $\langle 1\,0\,0\rangle$ loops. The two inserted platelets are initially separated a distance of $0.333a_0$ and $0.666a_0$ respectively, to minimize the atomic stress along the corresponding Burgers vector direction in the unrelaxed computation box. Upon subsequent low-temperature annealing, the clusters relax to the appropriate value of $b = a_0\sqrt{3}/2$ for $\frac{1}{2}\langle 1\,1\,1\rangle$ and $b = a_0$ for $\langle 1\,0\,0\rangle$ loops. The resulting $\frac{1}{2}\langle 1\,1\,1\rangle$ loops are perfect, intrinsically kinked (they distribute over multiple $\{1\,1\,0\}$ planes), very mobile and most stable with respect to any other SIA clusters in *bcc* Fe [6,15]. The $\langle 1\,0\,0\rangle$ loops are perfect, lie mostly on a single pair of $\{2\,2\,0\}$ planes and have a significantly reduced mobility relative to the $\frac{1}{2}\langle 1\,1\,1\rangle$ loops, with an activation barrier for migration, $E^{\mathrm{m}} > 2.5$ eV [9].

Perfect $\langle 1\,0\,0\rangle\{1\,0\,0\}$ loops were generated by using the above procedure, but repeated in two consecutive $\{1\,0\,0\}$ planes to assure that the stacking fault is removed and that the normal stacking sequence along the $[1\,0\,0]$ direction, *ABAB*, is conserved. In this case, the close-packed directions are $\langle 1\,0\,0\rangle$ so the loops are square or rectangular shape with sides along $\langle 1\,0\,0\rangle$ directions. As for the $\langle 1\,0\,0\rangle$ $\{1\,1\,0\}$ case, $\langle 1\,0\,0\rangle$ $\{1\,0\,0\}$ loops, although perfect edge in nature, have a very low mobility and remain on the original *AB* $\{1\,0\,0\}$ habit planes.

4. Results and discussion

Fig. 1 shows the formation energy vs. size curves for the three types of loops considered, calculated from a fit of the continuum elasticity theory expressions given by Hirth and Lothe [18] to our atomistic results. As pointed out before, $\frac{1}{2}\langle 1\,1\,1\rangle$ loops are the most stable under any circumstance, although the energy difference

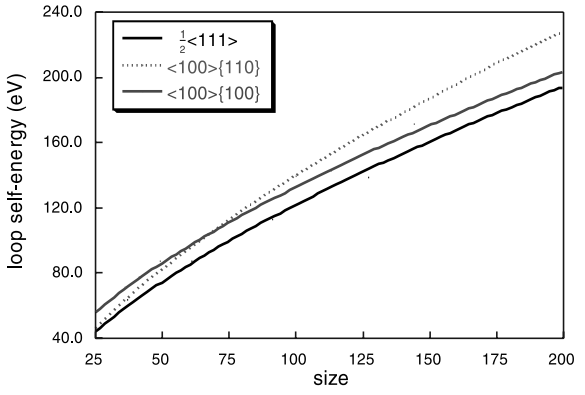

Fig. 1. Dislocation loop energy as a function of size (number of constituent interstitials) for $\frac{1}{2}\langle 1\,1\,1\rangle\{1\,1\,0\}$, $\langle 1\,0\,0\rangle\{1\,1\,0\}$ and $\langle 1\,0\,0\rangle\{1\,0\,0\}$ *magic* clusters. The curves have been obtained as MD data fits to the continuum elasticity expressions given in Ref. [17]. Up to the sizes considered, $\frac{1}{2}\langle 1\,1\,1\rangle$ are always more stable than $\langle 1\,0\,0\rangle$ loops. These lie originally on $\{1\,1\,0\}$ planes, until about sizes 65–70, when they change habit planes to $\{1\,0\,0\}$.

with respect to $\langle 1\,0\,0\rangle$ $\{1\,0\,0\}$ becomes very small with increasing loop sizes (e.g., ~13 eV for a loop containing 127 self-interstitials). Initially, $\langle 1\,0\,0\rangle$ loops are more stable on $\{1\,1\,0\}$ planes but, as size increases, $\langle 1\,0\,0\rangle\{1\,0\,0\}$ configurations become energetically favored. This is believed to stem from the significant reduction of dislocation segment length that $\langle 1\,0\,0\rangle$ loops undergo when rotating from $\{1\,1\,0\}$ to $\{1\,0\,0\}$ planes. The critical size for habit plane rotation is estimated to be around 70. We have also tried loop configurations that do not comply with the above guidelines, such as hexagonal $\langle 1\,0\,0\rangle\{1\,0\,0\}$, square $\langle 1\,0\,0\rangle\{1\,1\,0\}$ and rhombic $\frac{1}{2}\langle 1\,1\,1\rangle\{1\,1\,0\}$ clusters. In all cases the formation energies for these defects were higher than for the magic loops.

Fig. 2 shows the CTEM simulated images of a 91-SIA, hexagonal, $\frac{1}{2}\langle 1\,1\,1\rangle\{1\,1\,0\}$ loop and a 61-SIA, hexagonal, $\langle 1\,0\,0\rangle\{1\,0\,0\}$ loop, taken under the above conditions. A cut perpendicular to the [0 0 1] direction of the simulation box for each loop is also shown. The observed contrast in the images originates from the defect-induced displacement field. From the images, it is clear that the displacement field caused by the $\frac{1}{2}\langle 1\,1\,1\rangle$ loop is mostly circumscribed to the glide prism of the defect, while on the contrary, for the $\langle 1\,0\,0\rangle$, the strain field has stereoscopic geometry and reaches outside the glide prism of the loop. This is likely a consequence of the larger dislocation core volume for $\langle 1\,0\,0\rangle$ interstitial loops, whereas the compressive stress caused by $\frac{1}{2}\langle 1\,1\,1\rangle$

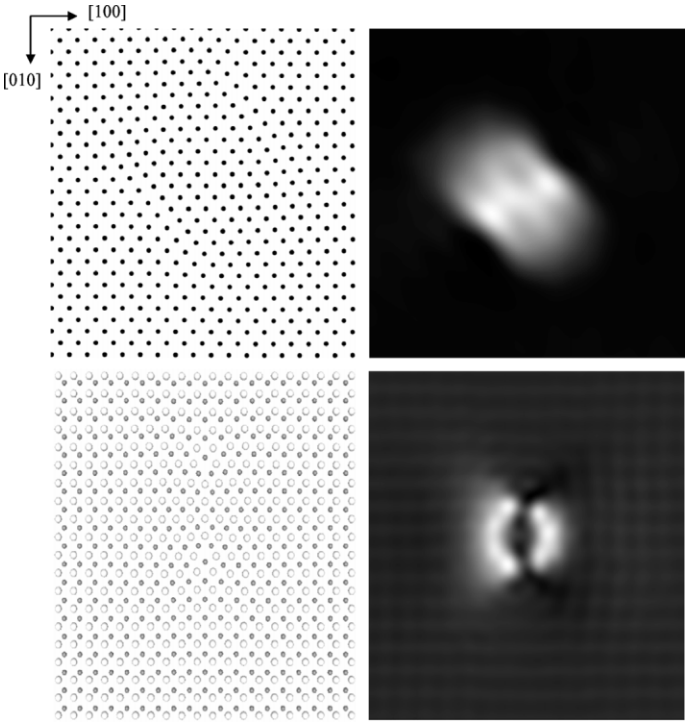

Fig. 2. [0 0 1] view of the MD simulation box after relaxation of a $\frac{1}{2}[1\,\bar{1}\,1]$ (top image) and a [1 0 0] (bottom) loop respectively. Next to each one of the atomistic images are the corresponding weak beam, $\mathbf{g} = (2\,0\,0)$, $\mathbf{g}(4.1\mathbf{g})$, CTEM simulated images.

loops is more easily accommodated along close-packed $\langle 1\,1\,1\rangle$ directions, with even small tensile regions appearing in between the main twin compressive lobes of the individual crowdions that constitute the cluster [19]. This means that the displacement field induced by the loops in the direction perpendicular to the Burgers vector is virtually non-existent, although this is not so clearly appreciated in the image of the $\frac{1}{2}\langle 1\,1\,1\rangle$ loop, since the diffraction vector is not parallel to the Burgers vector ($\mathbf{b}\times\mathbf{g}\neq 0$). Another interesting feature is that while the $\langle 1\,0\,0\rangle$ loop clearly lies on two consecutive *AB* $(2\,0\,0)$ planes (to conserve the stacking sequence *ABAB*), the $\frac{1}{2}\langle 1\,1\,1\rangle$ rests on several $(1\,\bar{1}\,0)$ planes through kinks that are weakly distinguishable in the image. The double-*bean* contrast observed in the $\langle 1\,0\,0\rangle$ image is characteristic of interstitial dislocation loops in metals, irrespective of their Burgers vector. This includes $\frac{1}{2}\langle 1\,1\,1\rangle$ clusters in Fe, as recognized in several experiments where $\frac{1}{2}\langle 1\,1\,1\rangle$ loops were observed edge-on ($\mathbf{b}\times\mathbf{g}=0$) [2].

The shape of the dislocation loops does not seem to have a significant effect on the simulated images, although it significantly influences the loop self-energies. Fig. 3 shows a series of $\langle 1\,0\,0\rangle\{1\,1\,0\}$ loops of different sizes and their associated weak-beam images, which indicates that little information about the shape of the loops can be extracted using this set of CTEM imaging conditions. The images are qualitatively similar to that of the previous $\langle 1\,0\,0\rangle\{1\,0\,0\}$ loop of Fig. 2, with the double-bean contrast clearly observed in all cases.

The results for loop energetics shown in Fig. 1 agree well with experiments [1,4] in that, for sizes larger than 65–70 SIAs, $\langle 1\,0\,0\rangle$ loops are most stable on $\{1\,0\,0\}$ planes. For the purpose of directly comparing the simulated images with actual TEM micrographs, an irradiated tempered martensite steel sample was analyzed in the microscope. Fig. 4 shows an experimental TEM, weak beam, $\mathbf{g}(4.1\mathbf{g})$, $\mathbf{g}=(2\,0\,0)$ image of a F82H (Fe–9Cr) tempered martensite steel sample. The material was neutron irradiated at high dose rate and 302 °C, up to a total dose of 8.8 dpa in the HFR facility in Petten. The observed microstructure contains a number of features, most of which are defect clusters generated by the irradiation. The two insets displayed in Fig. 4 represent an 18 nm long, 937-SIA, rectangular, $\langle 1\,0\,0\rangle$ $\{1\,0\,0\}$ loop (A – bottom right) and a 4 nm, 91-SIA, hexagonal, $\langle 1\,0\,0\rangle$ $\{1\,0\,0\}$ loop (B – top left). Both loops exhibit characteristics that can be qualitatively recognized in the experimental micrograph, where two defects with similar size and contrast have been pointed out (A and B). These are interstitial dislocation loops with $\langle 1\,0\,0\rangle$ Burgers vector and lying on $\{1\,0\,0\}$ planes. We emphasize the excellent agreement between the simulations and the experimental observations, although it is important to note that this example is for a single imaging condition.

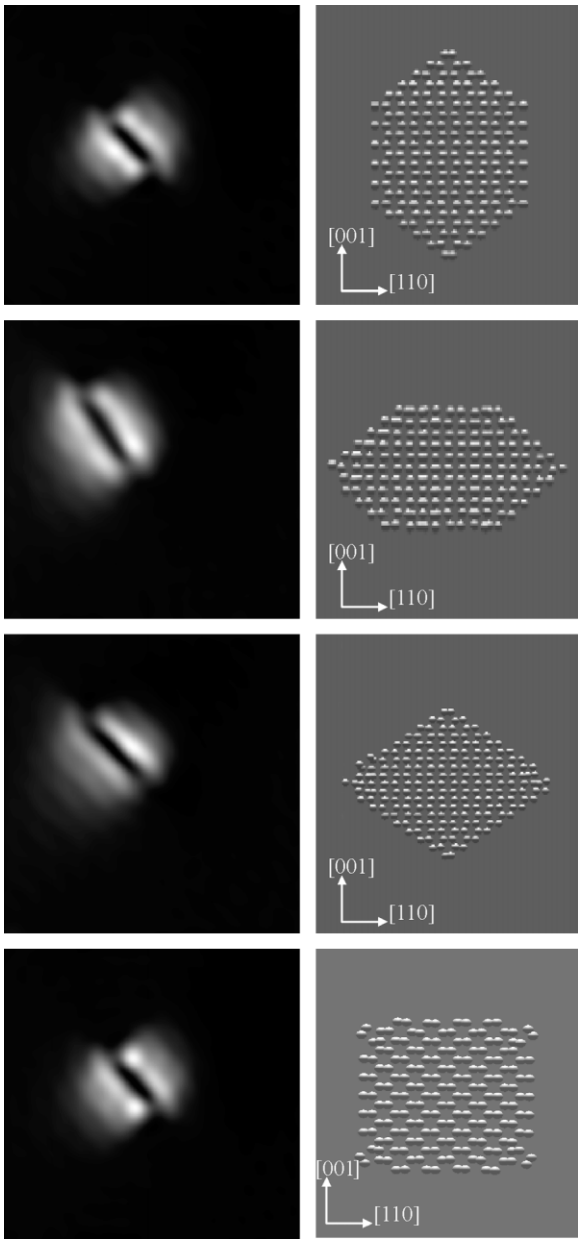

Fig. 3. CTEM simulated images (left) of $\langle 1\,0\,0\rangle\{1\,1\,0\}$ loops with different sizes and shapes (right). The atomic configurations on the right are viewed from a $[1\,\bar{1}\,0]$ direction.

5. Summary and conclusions

The results presented in this paper show that the image simulation technique can be successfully applied to help close the gap between atomistic MD computer simulations and the experimental results in α-Fe deduced from TEM. We have performed an energetics analysis for the two types of loops that are known to

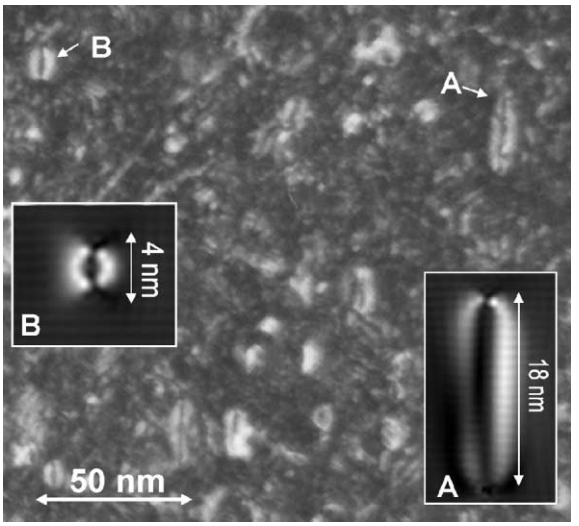

Fig. 4. Experimental TEM weak beam image of a Fe–9Cr crystal irradiated with neutrons to a dose of 8.8 dpa at 302 °C. The two insets represent CTEM simulated images of (A) an 18 nm, rectangular [1 0 0] loop and (B) a 4 nm, hexagonal, [1 0 0] loop. A number of features can be observed in the TEM micrograph, among which two (A and B) interstitial loops with Burgers vector [1 0 0], sitting on {1 0 0} planes, can be identified. The agreement with the simulated loops in both contrast and shape is excellent.

exist in ferritic materials, those with Burgers vector $\frac{1}{2}\langle 1\,1\,1\rangle$ and those with $\langle 1\,0\,0\rangle$. $\langle 1\,0\,0\rangle$ loops are always metastable with respect to $\frac{1}{2}\langle 1\,1\,1\rangle$ loops, although the energy difference decreases as the loops become larger. $\langle 1\,0\,0\rangle$ clusters initially prefer $\{1\,1\,0\}$ habit planes, rotating to $\{1\,0\,0\}$ planes with increasing size.

Weak beam, CTEM images for a number of loops of different Burgers vectors, habit planes, sizes and shapes, using an image condition of $\mathbf{g} = (2\,0\,0)$ and $\mathbf{g}(4.1\mathbf{g})$ have been generated. Useful information about the induced strain field can be extracted from the CTEM simulated images in each case. The observed strain field of $\frac{1}{2}\langle 1\,1\,1\rangle$ loops remains mostly confined to the loop glide prism whereas that of $\langle 1\,0\,0\rangle$ clusters extends beyond the limits of the prism, with the CTEM image conditions chosen. Loop shape does not have any significant impact on the simulated images, which all exhibit the well known, double-bean contrast of SIA loops.

Finally, qualitative agreement between the simulated images and actual experimental micrographs taken from one specific experiment of a Fe–9Cr sample is found to be excellent, which validates the use of this technique to identify the nature of interstitial clusters in irradiated ferritic materials.

Acknowledgements

The authors are grateful to J.W. Rensman of the HFR facility at Petten, for providing the Fe–9Cr specimen for the TEM analysis. This work has been performed under the auspices of the US Department of Energy and Lawrence Livermore National Laboratory under contract W-7405-Eng-48 and within the CSN-UNESA Coordinated Research Programme under contract P000531499.

References

[1] D.S. Gelles, M.L. Hamilton, R. Schäublin, in: S.T. Rosinski, M.L. Grossbeck, T.R. Allen, A.S. Kumar (Eds.), Effects of Radiation on Materials: 20th International Symposium, ASTM STP 1405, American Society for Testing and Materials, West Conshohocken, PA, 2002.
[2] A.E. Ward, S.B. Fisher, J. Nucl. Mater. 166 (1989) 227.
[3] B.C. Masters, Philos. Mag. 11 (1965) 881.
[4] E.A. Little, R. Bullough, M.H. Wood, Proc. R. Soc. Lond. A 372 (1980) 565.
[5] A.C. Nicol, M.L. Jenkins, M.A. Kirk, Mater. Res. Soc. Symp. 650 (2001) R1.3.
[6] Y.N. Osetsky, A. Serra, B.N. Singh, S.I. Golubov, Philos. Mag. A 80 (2000) 2131.
[7] D.J. Bacon, T. Díaz de la Rubia, J. Nucl. Mater. 216 (1994) 275.
[8] N. Soneda, T. Díaz de la Rubia, Philos. Mag. A 78 (1998) 995.
[9] J. Marian, B.D. Wirth, J.M. Perlado, Phys. Rev. Lett. 88 (2002) 255507.
[10] D.J.H. Cockayne, I.L.F. Ray, M.J. Whelan, Philos. Mag. A 20 (1969) 1265.
[11] J.M. Cowley, A.F. Moodie, Acta Crystallogr. 10 (1957) 609.
[12] P.A. Stadelmann, Ultramicroscopy 21 (1987) 131.
[13] W.M. Stobbs, C.H. Sworn, Philos. Mag. 24 (1971) 1365.
[14] R. Schäublin, A. Almazouzi, Y. Dai, Y.N. Osetsky, M. Victoria, J. Nucl. Mater. 276 (2000) 251.
[15] B.D. Wirth, G.R. Odette, D. Maroudas, G.E. Lucas, J. Nucl. Mater. 276 (2000) 33.
[16] T. Díaz de la Rubia, M.W. Guinan, Mater. Res. Forum 174 (1990) 151.
[17] G.J. Ackland, D.J. Bacon, A.F. Calder, T. Harry, Philos. Mag. A 75 (1998) 713.
[18] J.P Hirth, J. Lothe, in: Theory of Dislocations, 2nd Ed., Krieger Publishing, 1982, p. 168.
[19] J. Marian, B.D. Wirth, J.M. Perlado, G.R. Odette, T. Díaz de la Rubia, Phys. Rev. B 64 (2001) 094303.